Ornithine Decarboxylase Antizyme Upregulates DNA-Dependent Protein Kinase and Enhances the Nonhomologous End-Joining Repair of DNA Double-Strand Breaks in Human Oral Cancer Cells†

Takanori Tsuji,‡ Miki Katsurano,‡ Soichiro Ibaragi,‡,§ Kaori Shima,‡ Akira Sasaki,§ and Guo-fu Hu*,‡

Department of Pathology, Harvard Medical School, Boston, Massachusetts 02115, and Department of Oral and Maxillofacial Surgery, Okayama University Graduate School of Medicine, Dentistry and Pharmaceutical Sciences, Okayama 700-8525 Japan

Received January 7, 2007; Revised Manuscript Received May 22, 2007

ABSTRACT: Ornithine decarboxylase (ODC) antizyme targets ODC for ubiquitin-independent proteosome degradation, thereby inhibiting polyamine synthesis. It has been shown to regulate DNA methylation and has tumor suppressor activity. Increasing evidence suggested that antizyme may also have ODC-independent functions. Here, we report that antizyme plays a role in DNA double-strand break repairs. A zinc-inducible human antizyme gene expression vector was transfected into UM1 human oral squamous cancer cells that do not express endogenous antizyme. The resultant upregulated genes were screened by cDNA arrays and confirmed by quantitative real-time polymerase chain reaction. DNA-dependent protein kinase including its catalytic subunit DNA−PKcs and regulatory subunit Ku70, two key proteins of the DNA damage repair machinery, was significantly upregulated after ectopic expression of antizyme. Consistently, we found that UM1 cells are sensitive to γ irradiation and deficient in DNA damage repairs, as shown by radio-sensitivity and Comet assays. Ectopic expression of antizyme increased radio-resistance of UM1 cells and restored their capacity of DNA damage repairs to the level of UM2 cells that have an identical genetic background but express endogenous antizyme. Plasmid end-joining assays confirmed that antizyme enhances the ability of UM1 cells to repair DNA double-strand breaks by the nonhomologous end-joining pathway.

Ornithine decarboxylase (ODC) catalyzes decarboxylation of L-ornithine to form putrescine and is the rate-limiting enzyme in the polyamine biosynthesis pathway. Enhanced ODC activity (*1*−*4*) and elevated polyamine levels (*5*) have been reported in a variety of human cancers. Inhibition of ODC activity and polyamine depletion by α-difluoromethylornithine have been shown to inhibit cell proliferation and induce terminal differentiation of F9 teratocarcinoma cells, accompanied by global DNA hypomethylation (*6*). ODC activity is negatively regulated by ODC antizyme (*7*), an intracellular protein that targets ODC for ubiquitin-independent proteasomal degradation. Four antizyme isoforms have been identified (*8*). Antizyme 1 is ubiquitously expressed. It binds reversibly to ODC, inhibits its activity, and targets it for degradation by 26S proteasomes (*9*). Antizyme 2 also has a wide tissue distribution, binds to ODC, and inhibits its activity but lacks the function to mediate protein degradation (*10*). Antizyme 3 is testis-specific and expressed only during late spermatogenesis (*11*, *12*). Antizyme 4 was identified as a sequence tag with unknown tissue distribution (*8*). Antizyme expression is regulated at the translational level by a +1 frame-shifting mechanism controlled by polyamines (*13*). Antizyme activity is also regulated at the protein level by an antizyme inhibitor protein that competes with ODC for antizyme binding (*14*).

We have shown that downregulation of antizyme is associated with cancer progression in the hamster buccal pouch carcinogenesis model (*15*). Ectopic expression of the antizyme gene in HCPC-1 hamster malignant oral keratinocytes results in DNA demethylation at the cytosine residues of the CCGG regions, leading to cell differentiation and reversal of the malignant phenotype (*16*). Moreover, overexpression of antizyme in transgenic mice suppresses skin tumor growth (*17*). These results indicate that antizyme has a tumor-suppressor function. However, it is unclear how antizyme exerts its tumor-suppressor function. Expressions of both ODC and antizyme are cell-cycle-dependent. In normal human fibroblasts, ODC expression decreases in the G_1 phase and increases in the S phase, whereas antizyme expression increases in the G_1 phase but decreases in the S phase (*18*). Thus, antizyme may have ODC-independent functions. Indeed, antizyme has been shown to inhibit cyclin D1 in an ODC-independent manner (*19*, *20*).

To better understand the role that antizyme plays in human cancer, we attempted to identify human genes that are upregulated by ectopic expression of human antizyme. We first surveyed a number of normal and malignant human oral keratinocyte lines for antizyme expression and found that

† This work was supported by NIH Grant CA100044 to T.T. and CA105241 to G.-f.H.

* To whom correspondence should be addressed: Department of Pathology, Harvard Medical School, 77 Avenue Louis Pasteur, Boston, MA. E-mail: guofu_hu@hms.harvard.edu. Telephone: 617-432-6582. Fax: 617-432-6580.

‡ Harvard Medical School.

§ Okayama University Graduate School of Medicine, Dentistry and Pharmaceutical Sciences.

10.1021/bi7000328 CCC: $37.00
Published on Web 07/14/2007

the UM1 human oral squamous cancer cells do not express detectable amounts of endogenous antizyme proteins, whereas the UM2 cells have a significant level of antizyme expression. UM1 and UM2 cells were isolated from the same tongue cancer lesion and have an identical genetic background. Both UM1 and UM2 cells form tumor burdens when they are injected into nude mice subcutaneously. However, when they were injected intravenously, only UM1 cells are able to form metastatic nodules in distant organs (*21*). Therefore, we chose these two human cell lines to study the effect of ectopic expression of human antizyme. A cDNA array screening approach was used to identify genes upregulated by antizyme. To focus on the genes that are potentially regulated via DNA demethylation, we compared the gene expression profile of antizyme overexpression with that of 5-Aza-2′-deoxycytidine (5-Aza-CdR) treatment. 5-Aza-CdR is a demethylating reagent that is incorporated into replicating DNA, rendering the DNA refractory to methylation (*22*, *23*). It has been widely used to uncover methylation-silenced genes. We thought that the outcome of 5-Aza-CdR treatment would provide a dataset that can be used to identify those genes whose expression is altered by antizyme possibly through DNA demethylation. A subset of genes that are commonly upregulated by antizyme and 5-Aza-CdR has been identified. However, sequence analyses did not reveal any CpG islands in the promoter regions of these genes. Thus, our approach failed to identify antizyme-induced gene upregulation through DNA demethylation. Instead, we found that antizyme upregulates the expression of G_1 genes involved in cell-cycle checkpoint and DNA damage repair processes. Therefore, we examined the sensitivity of UM1 cells to γ irradiation and their ability to repair DNA double-strand breaks before and after antizyme transfection. We found that UM1 cells are sensitive to γ irradiation and are deficient in DNA damage repair as compared to UM2 cells. Transfection of antizyme increases the radio-resistance and DNA damage repair ability of UM1 cells to a level comparable to that of UM2 cells.

MATERIALS AND METHODS

Cell Culture. Human normal oral keratinocyte lines OKF4 and OKF6 and human oral squamous cell carcinoma lines SCC4, SCC15, SCC66, and SCC105L were provided by J. Rheinwald (Brigham and Women's Hospital). They were cultured in keratinocyte−SFM supplemented with 50 μg/mL bovine pituitary extract and 0.1 ng/mL epidermal growth factor (EGF). UM1 and UM2 human oral squamous cell carcinoma cells (*21*) were cultured in Dulbecco's modified eagle medium (DMEM)/F-12 plus 10% fetal bovine serum (FBS).

Transfection of UM1 Cells with Antizyme cDNA. The zinc-inducible human wild-type antizyme 1 gene expression vector (pMT/CB6$^+$HuFSAZ-wt) was provided by S. Mizutani (*24*). This vector and the control vector pMT/CB6$^+$ were transfected into UM1 cells by a Gene-Gun (Bio-Rad) at 150 psi. Stable transfectants were selected with 1 mg/mL of G418 for 2 weeks. Antizyme expression was induced by the treatment of the cells with 100 μM $ZnSO_4$ for 5 days.

Cell-Cycle Analysis. The UM1 parent cells, vector and antizyme transfectants, and UM2 cells were cultured in the presence of 100 μM $ZnSO_4$ for 5 days to 60−70% confluence, trypsinized, and fixed in ice-cold ethanol. After the DNA was stained with propidium iodide, the cells were analyzed for cell-cycle position with a FC500 flowcytometer (Beckman-Coulter).

cDNA Array Screening. Total RNA was isolated by the Chirgwin method (*25*). Radiolabeled cDNA probes were synthesized from 10 μg of total RNA with a gene-specific primer mixture containing primers for all spotted genes (BD Biosciences Clontech) as described in the protocol of the manufacturer. cDNA probes synthesized from the total RNA of the experimental and control groups were hybridized in parallel to an identical set of BD Atlas Human 3.6 Array membranes. After hybridization and washes, the membranes were exposed and the screens were scanned with a phosphorimager (Molecular Dynamics).

Array Data Analysis. The AtlasImage 2.7 analysis software was used to identify differentially expressed genes. The default external method was used for background calculation to adjust the signal intensities of the two membranes. The global normalization method (sum method) was employed in which the experimental array was normalized with respect to the control array based on the combined signal intensities of the entire membranes. A normalization coefficient was calculated and applied to the background-adjusted intensity of each gene. A threshold of 2-fold difference in the adjusted, normalized intensities was used to determine whether or not a gene is differentially expressed.

Quantitative Real-Time Polymerase Chain Reaction (qRT-PCR). qRT-PCR was performed to verify the results of cDNA array screening. The group of genes that are upregulated by both ectopic antizyme expression and 5-Aza-CdR treatment were analyzed. The first strand cDNA was synthesized from the same RNA samples that have been used for the cDNA array experiments. The PCR primers were designed using MacVector version 7.2 software based on the cDNA sequences that were downloaded from the NCBI database according to the GenBank accession numbers provided with the array membranes. The qRT-PCR reactions were performed using a LightCycler with LightCycler FastStart DNA Master SYBR Green I kit. Amplification of sample cDNA was monitored with the fluorescent DNA-binding dye SYBR Green in combination with an ABI 5700 sequence detection system. β-actin was used as an endogenous control for normalization. The PCR primer sequences, optimal annealing temperatures, and amplicon sizes are listed in Table 1.

Radio-Sensitivity Assay. The sensitivity of cells to γ irradiation was performed according to Asaumi et al. (*26*). Cells were cultured in triplicates and were irradiated at a dose ranging from 0 to 12 Gy. A total of 3 days after irradiation, cells were fixed with 4% formaldehyde solution in phosphate-buffered saline (PBS), stained with 10% Gimsa solution, and counted.

Comet Assay. A commercial CometAssay kit (R&D Systems) was used to measure DNA fragmentation (*27*). The assay was carried out in neutral condition that allows for the detection of mainly DNA double-strand breaks (*28*). Cells were adjusted to a density of 1×10^5 cells per mL and were mixed with melted LM agarose at 37 °C at a ratio of 1:10 (v/v). A 75 μL of the mixture was applied onto a CometSlide. The slides were placed in prechilled lysis solution, incubated for 30 min at 4 °C, and washed by immersing in 50 mL of

Table 1: List of PCR Primers for qRT-PCR

genes and primer sequences	annealing T (°C)	amplicon size (nt)
actin	56	146
forward: 5′-TGAAGGTGACAGCAGTCGGTTG-3′		
reverse: 5′-GGCTTTTAGGATGGCAAGGGAC-3′		
alkaline phosphatase, placental type 3 precursor	57	118
forward: 5′-TCACCAGGGGGATTTTGACAC-3′		
reverse: 5′-GAAGTTGAGATTTGGGGCAAGC-3′		
α-actinin 1	57	177
forward: 5′-GGAGTTCAAAGCCTGCCTCATC-3′		
reverse: 5′-TGGTCTGCTGTATCTGTGTCGG-3′		
amyloid-like protein 2	53	143
forward: 5′-ATACAGATGAGGGTGTCCGCTG-3′		
reverse: 5′-ATAGTTGGAAGGGGAAGTGAACG-3′		
antioxidant protein 2, AOP2	54	135
forward: 5′-TGGCAAGAAATACCTCCGCTAC-3′		
reverse: 5′-GCTGTGATGACACCAGGATGTG-3′		
antizyme inhibitor	53	335
forward: 5′-GCAACAACTGTCAGGTTAGTGATGC-3′		
reverse: 5′-TTTGAATAAACTTGGGGGGAGG-3′		
ATP-dependent DNA helicase II, 70 kDa subunit, Ku70	58	197
forward: 5′-AGAGTGGTCTGAAGAAGCAGGAGC-3′		
reverse: 5′-GCCTCAAAAACATAAAGTCCCTCG-3′		
calcium-binding protein p22; calcium-binding protein CHP	54	124
forward: 5′-GAGGGAGAGGACCAGGTAAACTTC-3′		
reverse: 5′-TGTTGCTTCGGCTGTTGAGTG-3′		
clathrin heavy subunit 1, CLH-17; KIAA0034	52	149
forward: 5′-AGAAGATTATCAGGCTCTGCGAAC-3′		
reverse: 5′-TCTGTTTCCAGCGATTGTTGC-3′		
cyclin-dependent kinase regulatory subunit 1, CKS1	52	107
forward: 5′-GAGGAAGCATCTGAGTTTGAGACC-3′		
reverse: 5′-CATAAATCCGCAAGTCACCACAC-3′		
cytochrome P450 IB1, CYP1B1	52	131
forward: 5′-TTATGTCAACCAGGTCCAGATGTG-3′		
reverse: 5′-AGCCAGGTAAACTCCAAGCACC-3′		
DNA-dependent protein kinase catalytic subunit, DNA−PKcs	55	156
forward: 5′-CAAGTGAAGTGCCTGATGGACC-3′		
reverse: 5′-TGGAATGCTGCCAACCAAAG-3′		
DNA fragmentation factor 40 kDa subunit, CAD, DFF40	54	246
forward: 5′-ATGGCAAGAAATAGGAAACCCC-3′		
reverse: 5′-TAGTAACGCTGACCAACGGAGC-3′		
DNA polymerase-α catalytic subunit	61	167
forward: 5′-CAAATGCTTCTCCAGCCATCC-3′		
reverse: 5′-ACCTGCTCAGTGTGTGTCTGTTGG-3′		
ephrin type A receptor 2 precursor, EphA2	57	143
forward: 5′-TATTCCCAAGCCGACCTTCC-3′		
reverse: 5′-ACCCAGTCAAGTTCACAGTCTGCC-3′		
ER lumen protein-retaining receptor 1; KDEL receptor 1; ERD 21	57	146
forward: 5′-TTCTGGCGTTCCTGGTCAATC-3′		
reverse: 5′-CAAGTAGTGGCTGGTGATGGTCTC-3′		
fascin; FX	60	175
forward: 5′-TGGAAACCCCAGAGAAAACGG-3′		
reverse: 5′-AAGAAAGAGGTGCCAGACTCGC-3′		
fos-related antigen, FRA1	57	100
forward: 5′-ACCACACCCTCCCTAACTCCTTTC-3′		
reverse: 5′-TGCTGCTGCTACTCTTGCGATG-3′		
G2/mitotic-specific cyclin B1	52	109
forward: 5′-GTCAAGAACAAGTATGCCACATCG-3′		
reverse: 5′-CAAGTTACACCTTTGCCACAGCC-3′		
heat-shock cognate 71 kDa protein	52	130
forward: 5′-TCCTTGGATGTCTGAGTGACCC-3′		
reverse: 5′-AACCCTTCTTTCTCCCTGACGC-3′		
intercellular adhesion molecule-1, ICAM-1	55	141
forward: 5′-TTCCCCCCAAAACTGACACC-3′		
reverse: 5′-AGGACAAGAGGACAAGGCATAGC-3′		
interferon-inducible RNA-dependent protein kinase (P68 kinase)	53	105
forward: 5′-TGGAAAGCGAACAAGGAGTAAGG-3′		
reverse: 5′-ATTAGCCCCAAAGCGTAGAGGTCC-3′		
KIAA0115	58	140
forward: 5′-CGGACAAGCCTATCACCCAGTATC-3′		
reverse: 5′-TGCTGAGTTGAAGTTGGAGTCGC-3′		
MAP kinase-activated protein kinase 2, MAPKAP kinase 2	57	155
forward: 5′-TGCTGAAGAGGCGGAAGAAAGC-3′		
reverse: 5′-AGAGGAGGCAGATGTGGACAGTTC-3′		

Table 1 (Continued)

genes and primer sequences	annealing *T* (°C)	amplicon size (nt)
minichromosome maintenance 4, MCM4 forward: 5′-AAAGGCTCCACAGAGGGAAGTGAG-3′ reverse: 5′-GGAAACACACCAAAGGAAGTGC-3′	56	297
minichromosome maintenance 5, MCM5 forward: 5′-ATGAGGAGAGGGATGTGATGCTGG-3′ reverse: 5′-ACTCGGCAGTAGGCAATAAACTTC-3′	56	130
minichromosome maintenance 7, MCM7 forward: 5′-TGTATCTCGTGGCTTCACACCC-3′ reverse: 5′-GCAGGCTGGAATCAGACAAAAG-3′	56	120
monocarboxylate transporter 1, MCT1 forward: 5′-AACTTTGGCAACATCTTGGCTG-3′ reverse: 5′-CTTTGAACAGGGGAGCAGAAATAG-3′	52	147
nonmetastatic protein 23B (NM23B) forward: 5′-CTACATTGACCTGAAAGACCGACC-3′ reverse: 5′-GCTGAAGGAGACTGCTGTTGTGTC-3′	57	337
proliferation cyclic nuclear antigen, PCNA forward: 5′-ACTAAGCTCTTTGAGAACTGCTTCTAAG-3′ reverse: 5′-TATTCTTTAAACAAATTGGAGAGAATAGAG-3′	53	151
protein−tyrosine phosphatase κ precursor forward: 5′-GGACATTCACCCTGGAAAGGAG-3′ reverse: 5′-GGTTTGATAACTTGACTCGCCG-3′	55	141
putative receptor protein, PM1 forward: 5′-TCTCCTGGCAGTTTGACCCTTG-3′ reverse: 5′-GTTTTGCTTCGCTCCCTGTTC-3′	57	238
pyruvate kinase M2 isozyme, PKM2 forward: 5′-TATTTGAGGAACTCCGCCGC-3′ reverse: 5′-CAGACTTGGTGAGGACGATTATGG-3′	58	123
replication factor C 37 kDa subunit, RFC37 forward: 5′-TGCCGAAGTTGACAAATGCC-3′ reverse: 5′-TTTACAAAACCCCCCATCCAG-3′	52	131
60S ribosomal protein L4, L1 forward: 5′-AACGATACGCCATCTGTTCTGCCC-3′ reverse: 5′-GCTTCCTTGGTCTTCTTGTAGCC-3′	54	142
60S ribosomal protein L22, RPL22 forward: 5′-CCCACCCTGTAGAAGATGGAATC-3′ reverse: 5′-TTGGAGAAAGGCACCTCGGATGTC-3′	55	163
skeletal muscle lim-protein 1, SLIM 1 forward: 5′-CATCAATAGGGAAGAGTGGTCC-3′ reverse: 5′-GCAGGGTTGCTTTTTGCTAAATGC-3′	52	130
sorcin 22 kDa protein, SRI; CP-22 forward: 5′-TGGCTGGAGACAACACTTTATCAG-3′ reverse: 5′-CCATTGGTGCTGTATCGTTTTGC-3′	53	147
thymosin β-4 forward: 5′-CGAAACTGAAGAAGACAGAGACGC-3′ reverse: 5′-AGAAGGCAATGCTTGTGGAATG-3′	54	140
transcription factor 11, TCF11; locus control region factor 1 forward: 5′-TGCTGTCCAAATACCAGTTGAGTG-3′ reverse: 5′-CACATCACGCTCCAGATTCAGG-3′	57	137
vascular endothelial growth factor precursor, VEGF forward: 5′-CTCAGAGCGGAGAAAGCATTTG-3′ reverse: 5′-TATGTGGGTGGGTGTGTCTACAGG-3′	58	489

TBE buffer. The slides were electrophoresed in TBE for 20 min at 15 V, rinsed with water, fixed with 70% ethanol for 5 min, stained with 50 μL of SYBR Green solution, and observed with a fluorescent microscope. A total of 80 cells in each group were photographed and analyzed. The outcome was analyzed using a TriTek CometScore software version 1.5.2.6 (http://autocomet.com). Tail moment was used in this study to measure the degree of DNA fragmentation.

Immunofluorescence of H2AX and Ku70. Cells were cultured on cover slips and fixed with methanol at −20 °C for 10 min, washed 3 times with PBS, and blocked with 10% FBS in PBS at pH 7.4 for 30 min at room temperature. Cells were then incubated with polyclonal rabbit anti-human phosphorylated histone H2AX (γ-H2AX) antibody (Trevigen) and monoclonal mouse anti-human Ku-70 antibody (Santa Cruz Biotechnology) at 1:100 dilution in PBS containing 10% FBS for 1 h, washed with PBS 3 times, and incubated with Alexa 555 goat F(ab′)$_2$ anti-rabbit IgG and Alexa 350 goat F(ab′)$_2$ anti-mouse IgG at 1:200 dilution in PBS for 1 h. The cover slips were mounted on glass slides and examined under a Leica DFC 480 fluorescent microscope.

Plasmid End-Joining Assay. A double-strand DNA break repair assay was performed according to the method by Zhong et al. (*29*) with modification. Red fluorescent protein was used instead of luciferase. A DNA fragment encoding red fluorescent protein was generated from a promoterless pDsRed2-1 vector by PCR with the primers: forward, 5′-ACG CGT CGA CAT GGC CTC CTC CGA GAA CGC-3′ containing a *Sal*I site; reverse, 5′-ATA AGA ATG CGG CCG CTC AGT TAT CTA GAT CCG GTG G-3′ containing a *Not*I site. This DsRed2 cDNA was cloned into the *Sal*I and *Not*I sites of the pCI-neo vector. The pCI-neo-DsRed2 was then digested with *Eco*RI between the CMV promoter

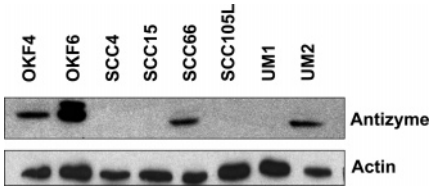

FIGURE 1: Antizyme protein levels in human normal and malignant oral keratinocytes. Cellular proteins from log-phase cells were extracted and analyzed by Western blotting (50 μg per lane) with a rabbit anti-rat antizyme polyclonal antibody (1:2000 dilution). Actin was blotted with a rabbit anti-actin polyclonal antibody (1:5000 dilution) as loading controls.

and DsRed2 coding sequence to linealize the plasmid. The linealized plasmid was transfected into the UM1 parent cells, vector and antizyme transfectants, and UM2 cells using a Gene-Gun. RFP expression was examined under a fluorescent microscope after 24 h of culture.

Differential Assay of Nonhomologous End-Joining (NHEJ) and Homologous Recombination (HR) Double-Strand DNA Break Repair. A plasmid-base DNA repair assay was used to differentiate the two major DNA repair processes (*30*). A linealized plasmid DNA (pREC, kindly provided by Dr. Takashi Kohno of the National Cancer Center Research Institute, Tokyo, Japan) containing two identical 400 bp inserts flanking the break point was transfected into the cells. The break-point junctions of the repaired plasmid DNA in the cells were analyzed by PCR to determine which repair processes have occurred. The pREC plasmid was double-digested with *Bsm*BI and *Eco*RV, and the linealized plasmid was transfected into the cells with a Gene-Gun (150 psi). Cellular DNA was collected from the transfectants 16 h post-transfection. PCR reactions were carried out using the Cy5-F1 and R2 primer set as described (*30*). This set of primers will amplify a DNA fragment of 3132 and 2488 bp, respectively, from the NHEJ and HR repair products of the linealized pREC (*30*).

RESULTS

Expression of the Antizyme Protein in Normal and Malignant Human Oral Keratinocytes. To identify a suitable human cell line for antizyme transfection, we measured the endogenous antizyme protein levels in a number of normal and malignant human oral keratinocyte lines by Western blotting. Figure 1 shows that the antizyme protein was detected in the OKF4 and OKF6 normal oral keratinocytes and in the SCC66 and UM2 oral squamous cell carcinoma lines but not in the SCC4, SCC15, SCC105L, and UM1 oral squamous cell carcinoma lines. Among these cells, UM1 and UM2 were isolated and established from the same primary tongue cancer region of a patient (*21*). The two cell lines have been cultured over 60 passages, and genetic analysis has revealed that they have identical genetic background (*21*). We therefore chose UM1 cells to study gene upregulation mediated by ectopic expression of antizyme.

Morphological Changes of UM1 Cells Induced by Ectopic Antizyme Expression. UM1 cells were transfected with the Zn-inducible human antizyme expression vector pMT/CB6$^+$-HuFSAZ-wt or with the control vector pMT/CB6$^+$. Stable transfectants were selected, and antizyme protein levels were determined by Western blotting analysis. As shown in Figure 2A, the antizyme protein was detected in the antizyme transfectants treated with 100 μM $ZnSO_4$ for 5 days. No corresponding band was detected in antizyme transfectants without $ZnSO_4$ treatment or in control vector transfectants both with and without $ZnSO_4$ treatment.

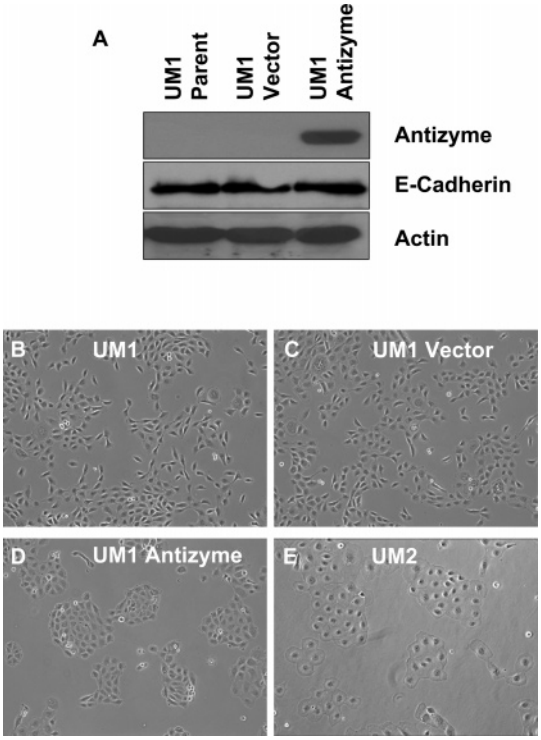

FIGURE 2: Effect of ectopic expression of antizyme on UM1 cell morphology. UM1 cells were transfected with antizyme expression vector pMT/CB6$^+$HuFSAZ-wt or control vector pMT/CB6$^+$. Stable transfectants were selected and cultured in the presence of 100 μM $ZnSO_4$ for 5 days. The antizyme and E-cadherin protein levels were analyzed by Western blotting (A). (B−E) Cell morphologies after 5 days of culture in the presence of 100 μM $ZnSO_4$.

Table 2: Antizyme Increases G1 Cell Population

cells	G1	S	G2
UM1	32.5 ± 1.8	39.6 ± 2.7	27.9 ± 1.0
UM2	46.8 ± 2.4	35.0 ± 2.0	18.2 ± 0.8
UM1, vector	37.0 ± 0.4	41.7 ± 0.3	21.3 ± 0.4
UM1, antizyme	52.0 ± 2.3	34.9 ± 0.5	13.1 ± 1.9

Induction of ectopic antizyme expression by 100 μM $ZnSO_4$ for 5 days resulted in the formation of epithelial island structures with tight cell−cell contacts (Figure 2D), similar to that seen in UM2 cells (Figure 2E). The vector control transfectants with $ZnSO_4$ treatment (Figure 2C) had a dispersed growth pattern without cell−cell adhesions, same as the UM1 parent cells (Figure 2B). Antizyme-induced morphological change is not mediated by E-cadherin because Western blotting showed that the E-cadherin protein level in UM1 cells was not altered by antizyme transfection (middle panel in Figure 2A).

Antizyme Induces G_1 Accumulation. Next, we examined the effect of antizyme expression on the cell-cycle distribution of UM1 cells. Table 2 shows that antizyme expression in UM1 cells increases G_1 cells from 37.0 to 52.0% with a concomitant decrease in both S and G_2 cells. The decrease in the G_2 phase (from 21.3 to 13.1%, representing a 38.5% decrease) is more dramatic than that in the S phase (from 41.7 to 34.9%, representing a 16.3% decrease). The cell-cycle distribution of UM1 antizyme transfectants is similar

Table 3: Genes Commonly Upregulated by 5-Aza-CdR Treatment and Antizyme Transfection

genes and classification	Genebank number	5-Aza-CdR[a]	antizyme[b]
cyclins, CDKs, CDK inhibitors, and intracellular kinases			
G2/mitotic-specific cyclin B1 (CCNB1)	M25753	3.5	3.4
cyclin-dependent kinase regulatory subunit 1 (CKS1)	X54941	4.0	3.9
MAP kinase-activated protein kinase 2	U12779	2.0	2.7
transcription factor 11 (TCF11); HBZ17	U08853	4.7	3.3
oncogenes and tumor suppressor			
fos-related antigen (FRA1); FOS-like antigen 1	X16707	61.6	22.3
nonmetastatic protein 23B (NM23B)	L16785/M36981	2.1	2.8
DNA polymerases, replication factors, and topoisomerases			
MCM4 DNA replication licensing factor	X74794	3.3	2.6
DNA replication licensing factor	X74795	2.0	2.0
DNA replication licensing factor	D55716	3.6	5.6
proliferating cyclic nuclear antigen (PCNA)	M15796	2.0	2.7
Ku 70 kDa subunit	M32865/S38729	3.4	4.6
DNA polymerase-α catalytic subunit (POLA)	X06745/J04718	2.1	3.4
activator 1 37 kDa subunit; RFC4	M87339	11.9	7.4
DNA damage repair proteins and ligases and DNA fragmentation proteins			
DNA−PK catalytic subunit (DNA−PKcs)	U35835	53.3	74.9
CAD; DNA fragmentation factor 40 kDa subunit (DFF40)	AF064019	2.0	3.5
death kinases intracellular kinase network members			
interferon-inducible RNA-dependent protein kinase	M35663/U50648	2.2	3.1
symporters and antiporters			
monocarboxylate transporter 1 (MCT1)	L31801	2.1	4.8
intracellular transducers, effectors, and modulators			
ephrin type A receptor 2 precursor, EphA2	M59371/M3639	8.0	9.8
matrix adhesion receptors			
intercellular adhesion molecule 1 precursor (ICAM1)	J03132	2.0	3.3
heat-shock proteins			
heat-shock cognate 71 kDa protein	Y00371	2.2	2.9
growth factors, cytokines, and chemokines			
vascular endothelial growth factor precursor	M32977/M2728	6.1	6.7
extracellular communication proteins			
thymosin β 4; FX	M17733	3.0	4.3
basic transcription factors			
skeletal muscle lim-protein 1 (SLIM 1) = (FHL-1)	U60115	8.6	7.3
trafficking and targeting proteins			
ER lumen protein-retaining receptor 1	X55885	2.2	2.1
calcium-binding protein p22	U61538	2.6	2.3
clathrin heavy subunit 1 (CLH-17); KIAA0034	D21260	2.5	2.0
complex carbohydrate metabolism			
KIAA0115	D29643	3.6	3.0
energy metabolism			
pyruvate kinase M2 isozyme (PKM2)	M23725	2.2	3.3
alkaline phosphatase, placental type 3 precursor	M14170	5.5	8.7
ribosomal proteins			
60S ribosomal protein L22 (RPL22)	X59357	3.4	3.7
60S ribosomal protein L4 (L1)	L20868	2.4	2.4
calcium-binding proteins			
sorcin 22 kDa protein (SRI); CP-22	L12387	4.2	4.9
other intracellular transducers, effectors, and modulators			
amyloid-like protein 2	S60099	2.6	2.4
protein phosphatase receptors			
protein−tyrosine phosphatase κ precursor	Z70660	4.4	4.0
G protein-coupled receptors			
putative receptor protein (PM1)	X51804	2.1	2.4
cytoskeleton and motility proteins			
α-actinin 1 cytoskeletal isoforms	X15804	12.2	6.7
fascin (actin-bundling protein)	U03057	2.1	3.1
xenobiotic, complex lipid and other metabolism			
cytochrome P450 IB1 (CYP1B1)	U03688	2.6	5.3
antioxidant protein 2 (AOP2)	D14662	6.5	5.5

[a] The ratio of the signal intensity between 5-Aza-CdR-treated cells and UM1 parent cells (5-Aza-Cdr/UM1). [b] The ratio of the signal intensity between antizyme and vector transfectants (antizyme/vector).

to that of the UM2 cells, suggesting that antizyme is responsible for the differential cell-cycle distribution between UM1 and UM2 cells. Student's *t* test indicated that the increases in G_1-phase cells of the UM1 antizyme transfectants with respect to the UM1 parent cells and the UM1 vector transfectants are significant ($p < 0.01$), whereas there is no significant difference in G_1 cell distribution between UM1 parent cells and vector transfectants and between UM1 antizyme transfectants and UM2 cells ($p > 0.05$).

Antizyme activity is known to be regulated at the protein level by the antizyme inhibitor (*31*). We therefore examined the expression level of the antizyme inhibitor by qRT-PCR. While the mRNA level of the antizyme inhibitor in UM2 cells is 39% of that in UM1 cells, antizyme transfection in

Table 4: Genes Whose Upregulation Has Been Confirmed by qRT-PCR

genes	antizyme/vector[a]	5-Aza/UM1[b]
DNA-dependent protein kinase catalytic subunit, DNA−PKcs	2.59 ± 0.39	8.22 ± 0.24
Ku 70 kDa subunit, Ku70	2.71 ± 0.56	80.09 ± 11.64
MCM4 DNA replication licensing factor	5.07 ± 1.17	64.88 ± 8.04
MCM5 DNA replication licensing factor	59.33 ± 0.14	13.58 ± 0.84
proliferating cyclic nuclear antigen, PCNA	3.64 ± 0.09	5.09 ± 0.11
DNA polymerase-α catalytic subunit, POLA	8.10 ± 0.12	1.81 ± 0.28
α-actinin	13.40 ± 0.61	22.66 ± 0.38
fascin	1.36 ± 0.06	2.72 ± 0.01
monocarboxylate transporter 1, MCT1	1.46 ± 0.15	2.22 ± 0.07
pyruvate kinase M2 isozyme, PKM2	4.65 ± 0.61	5.34 ± 0.13
ephrin type A receptor 2 precursor, EphA2	7.51 ± 0.04	1.97 ± 0.07
fos-related antigen, FRA1	1.89 ± 0.11	3.07 ± 0.10
vascular endothelial growth factor precursor, VEGF	2.06 ± 0.71	11.92 ± 1.60
ER lumen protein retaining receptor 1; KDEL receptor 1	12.30 ± 1.13	12.01 ± 0.51
dolichyl-diphosphooligosaccharide protein glycosyltransferase	1.75 ± 0.35	24.56 ± 0.70
60S ribosomal protein L	41.54 ± 3.03	16.31 ± 1.27
amyloid-like protein 2	2.31 ± 0.43	10.31 ± 0.19
alathrin heavy subunit 1, CLH-17	3.61 ± 0.52	7.57 ± 0.30

[a] The ratio of the signal intensity between antizyme and vector transfectants (antizyme/vector). [b] The ratio of the signal intensity between 5-Aza-CdR-treated cells and UM1 parent cells (5-Aza-Cdr/UM1).

UM1 cells do not change the expression level of the antizyme inhibitor. UM1 vector and antizyme transfectants have 95 ± 1.3 and 94 ± 1.7%, respectively, of the antizyme inhibitor mRMA level of the UM1 parent cells.

Genes Upregulated by Ectopic Antizyme Expression and 5-Aza-CdR Treatment. In an attempt to identify all of the methylation-silenced genes in UM1 cells, we treated the cells with 10 μM 5-Aza-CdR for 5 days, a condition known to demethylate cytosine residues and induce the re-expression of genes silenced by promoter methylation (*22*, *23*). Incorporation of 5-Aza-CdR into the replicating DNA renders the DNA refractory to methylation, thereby demethylating DNA genome wide. RNA was isolated from treated and untreated cells, and cDNA array analyses were performed. Detectable signals were obtained from about 40% of the 3528 genes spotted on the array membranes, a reasonable rate for this type of analysis. A gene is considered to be upregulated if its intensity (adjusted and normalized) in the experimental array is ≥2-fold stronger than that in the control array. Similarly, it is considered to be downregulated when its intensity is ≤50% of that in the control. This threshold factor of 2 is widely used in the field of array analysis (*32*−*36*). Using these criteria, we determined that 85 genes were upregulated and 94 genes were downregulated by 5-Aza-CdR treatment (data not shown). The same criteria were applied to antizyme and control vector transfectants. Ectopic antizyme expression resulted in the upregulation of 122 and downregulation of 173 genes (data not shown) in UM1 cells. Among the 122 genes whose expression is upregulated by antizyme, 39 were found also to be upregulated by 5-Aza-CdR treatment (Table 3).

Antizyme Upregulates G1-Phase-Related Genes. qRT-PCR were performed to verify the expression levels of the 39 genes identified above. Conventional RT-PCR reactions were carried out to confirm that the primer set (Table 1) was able to amplify single amplicons. With these primers, qRT-PCR analyses showed that 19 of the 39 genes were truly upregulated in antizyme transfectants (Table 4). While this was a disappointing success rate for the array screening approach, it is interesting to note that this list contains genes known to play a role in the G_1 transition, including DNA−PKcs, Ku70, MCM4, MCM5, PCNA, and DNA−polymerase-α.

Antizyme Enhances Resistance to γ Irradiation. Among the confirmed genes, DNA−PKcs and Ku70 are two essential proteins of the DNA damage repair machinery (*37*). We therefore examined the effect of antizyme on DNA damage repairs. First, we measured the sensitivity of UM1 cells to γ irradiation before and after antizyme transfection and compared it with that of UM2 cells. Irradiation is known to cause DNA double-strand breaks and DNA fragmentation which, if not properly repaired, induces apoptosis (*38*, *39*). UM1 parent cells, vector and antizyme transfectants, and UM2 cells were exposed to increasing doses of γ irradiation (0, 2, 4, 6, 8, 10, and 12 Gy). Survived cells were counted 3 days after irradiation. Figure 3 shows that UM1 parent cells and vector transfectants are more sensitive to irradiation damage than UM2 cells. Antizyme transfection increased radio-resistance of UM1 cells to a comparable level as that of UM2 cells.

Antizyme Reduces DNA Fragmentation in UM1 Cells. The Comet assay was carried out to quantify DNA damage in UM1 cells and the recovery after antizyme transfection. Cells were not pretreated, and the assay was performed in a neutral pH. Therefore, only the endogenous double-strand breaks were measured (*28*). As shown in Figure 4, extensive tail areas were observed in UM1 parent cells and vector transfectants (parts A and B of Figure 4). However, UM2 cells and the antizyme UM1 transfectants showed no significant comet tails (parts C and D of Figure 4). Tail moment that reflects the degree of damaged fragmentation was calculated from the tail length and the percentage of tail DNA. A total of 80 randomly selected cells from each group were evaluated using a TriTek CometScore software version 1.5.2. Mean tail moment of UM1 parent cells, vector and antizyme UM1 transfectants, and UM2 cells were 14.5 ± 5.7, 19.5 ± 3.6, 4.3 ± 1.3, and 2.5 ± 1.5, respectively (Figure 4E). Thus, antizyme transfection recovered the ability of UM1 cells to repair DNA double-strand break by 89% as compared to that of UM2 cells.

Antizyme Decreases γ-H2AX Foci Formation and Enhances Ku70 Recruitment. Histone γ-H2AX immunofluorescence was performed to determine the degree of double-

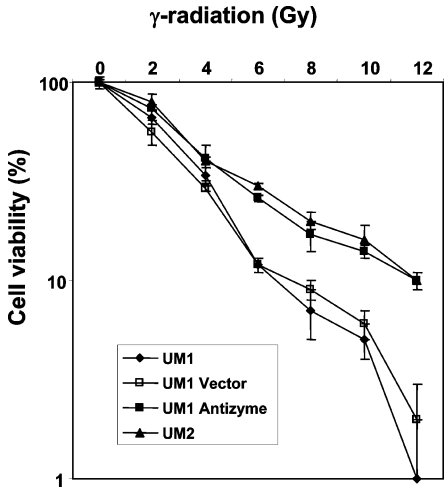

FIGURE 3: Antizyme increases the radio-resistance of UM1 cells. UM1 parent cells, vector and antizyme transfectants, and UM2 cells were cultured to 60−70% confluence in the presence of 100 μM Zn SO_4 and were exposed to γ radiation at the doses indicated. The cells were cultured for an additional 3 days and counted after being fixed with 4% formaldehyde and stained with 10% Gimsa solution. The percentage of cell viability was calculated using the number of cells from the dish without γ irradiation as 100%. Results shown were mean ± standard deviation (SD) of three independent experiments in triplicates.

strand DNA breaks in UM1 cells and the resultant changes after antizyme transfection. As shown in parts A−L of Figure 5, γ-H2AX was intensively stained in the nuclei of UM1 cells (Figure 5A) and in the vector control UM1 transfectants (Figure 5B). The intensity of staining was significantly reduced in antizyme UM1 transfectants (Figure 5C) and in UM2 cells (Figure 5D). In contrast, the staining intensity of Ku70 was much lower in UM1 cells (Figure 5E) and in the vector control UM1 transfectants (Figure 5F) than that in antizyme UM1 transfectants (Figure 5G) and in UM2 cells (Figure 5H). Figure 5M shows that the number of γ-H2AX foci per nucleus in UM1 and vector control UM1 transfectants was 95.2 ± 38.8 and 88.3 ± 28.0, respectively, which was reduced to 8.3 ± 7.6 after antizyme transfection and not significantly different from that in UM2 cells (9.9 ± 8.7). the merge of the red (γ-H2AX) and blue (Ku70) fluorescence showed that Ku70 is colocalized with g-H2AX (parts I−L of Figure 5). Quantitative analyses (Figure 5N) showed that only 20.8 ± 5.2 and 13.3 ± 0.4%, respectively, of the γ-H2AX foci were stained positively for Ku70 in UM1 and vector control UM1 transfectants. However, the percentage of Ku70 and γ-H2AX colocalization increased to 89.8 ± 2.8 and 84.2 ± 2.6%, respectively, in antizyme UM1 transfectants and in UM2 cells. These results confirmed the Comet assay (Figure 4) and indicate that double-strand DNA breaks occurred in UM1 cells to a significant degree and were not adequately repaired. UM1 antizyme transfection increased the expression level of Ku70, consistent with the array screening (Table 3) and the qRT-PCR results (Table 4) and enhanced the recruitment of KU70 to the double-strand DNA break lesions to promote DNA repair.

Antizyme Enhances End-Joining of DNA Double-Strand Breaks. Next, we carried out a DNA double-strand break end-joining assay to see whether antizyme overexpression enhances the ability of UM1 cells to repair DNA damage by the NHEJ pathway. A red fluorescent protein expression vector was constructed by inserting a cDNA encoding

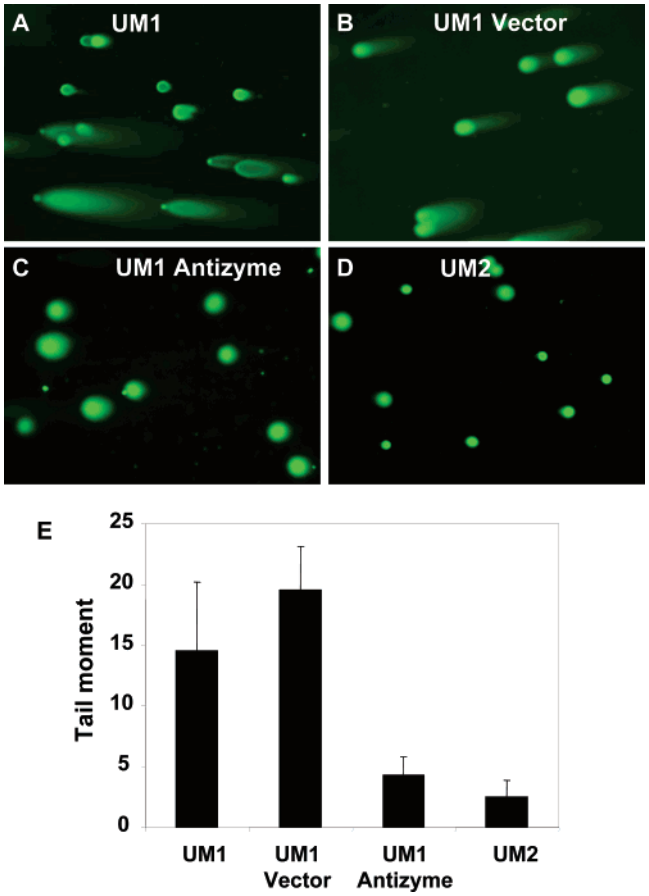

FIGURE 4: Antizyme decreases DNA damage in UM1 cells. UM1 parent cells (A), vector (B) and antizyme (C) transfectants, and UN2 cells (D) were cultured to 60−70% confluence and were collected with a rubber policeman. After Comet electrophoresis, DNA was stained with SYBR Green and analyzed using TriTek CometScore software, version 1.5.2.6. The tail length was defined as the distance of the edge of the head and the end of the tail. The DNA content in the entire comet was calculated by multiplying the area covered by the whole comet with the mean comet intensity. The DNA content of the head was measured by multiplying the area of the head with the mean head intensity. The DNA content of the tail is derived by subtracting the DNA content of the head from that of the whole comet. The percentage of DNA in the tail was calculated as (DNAT/DNAT + DNAH) × 100%. The tail moment (E) was calculated by multiplying the tail length with the percentage of DNA in the tail. Results shown are from a representative experiment of five repeats.

DsRed2 downstream of the CMV promoter of the pCI-neo vector (Figure 6A). This plasmid was then linealized by *Eco*RI digestion between the CMV promoter and DsRed2 coding region. Because DsRed2 is located upstream of the CMV promoter in the linealized DNA, it will not be expressed in cells before the double-strand break is rejoined (Figure 6A). This strategy has been used by Zhong et al. to determine the BRCA1-mediated end-joining activity of mouse embryonic fibroblasts (*29*). The linealized pCI-DsRed2 plasmid was transfected into UM1 and UM2 cells, as well as the vector and antizyme UM1 transfectants. As shown in parts B−E of Figure 6, no DsRed2 expression was detected in UM1 parent cells (Figure 6B) and in the vector UM1 transfectants (Figure 6C), indicating that UM1 cells lack the end-joining DNA double-strand repair activity. However, DsRed2 was expressed in ~25% of the cells in the antizyme UM1 transfectants (43.4 ± 5.9 cells per microscopic field) (Figure 6D) and in UM2 cells (55.5 ±

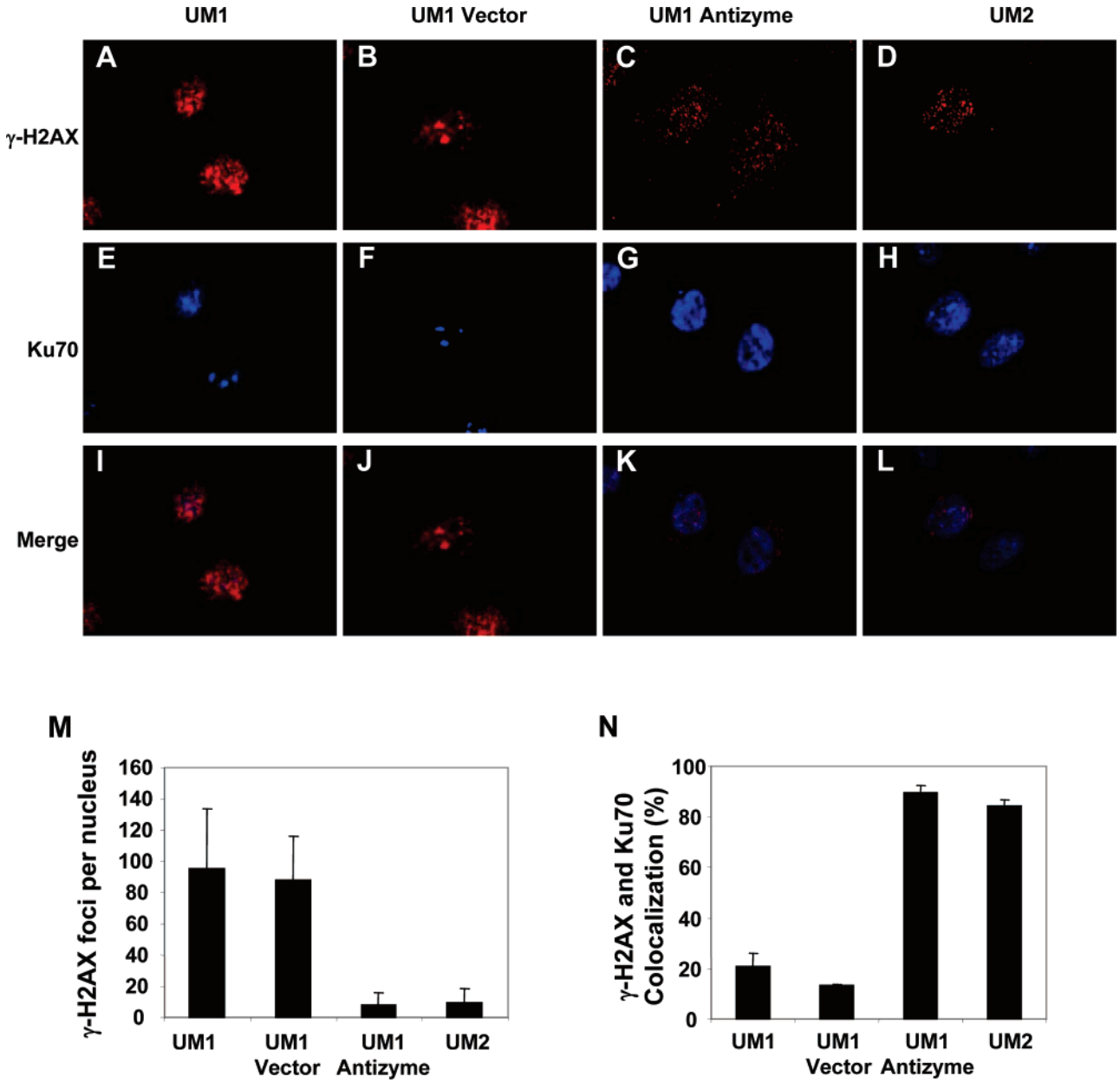

FIGURE 5: Antizyme decreases γ-H2AX foci formation and increases Ku70 expression and recruitment into the DNA break lesions. UM1 parent cells (A, E, and I), UM1 vector (B, F, and J) and antizyme (C, G, and K) transfectants, and UM2 cells (D, H, and L) were cultured in the presence of 100 μM $ZnSO_4$ for 5 days. The cells were double-stained for γ-H2AX (A−D) and Ku70 (E−H) with red and blue fluorescence, respectively. Colocalization of γ-H2AX and Ku70 was shown by merging the two colors (I−L). The γ-H2AX foci were counted under a fluorescent microscope at 1000 magnification from 30 randomly selected nuclei (M). The percentage of γ-H2AX and Ku70 colocalization was calculated from the number of foci showing overlapping blue and red fluorescence and the total number γ-H2AX foci of a given nucleus (N).

5.4 cells per microscopic field) (Figure 6E), indicating that antizyme expression enabled the cells to end-join the linealized plasmid. Cotransfection with a green fluorescent protein expression vector showed that the transfection efficiency was around ~25%. Image merging results indicated that all of the transfected cells have recovered the end-joining activity (data not shown). These results demonstrated that antizyme enhances the DNA double-strand breaks repair activity of the cells by the NHEJ pathway, consisting with the upregulation of DNA−PKcs and Ku70 (Table 4).

To determine whether antizyme also enhances the HR DNA repair pathway, we transfected linealized pREC into the cells and used PCR to differentiate HR from NHEJ (*30*). Figure 7A illustrates that NHEJ and HR repair processes will result in a circularized plasmid of different size. Accordingly, PCR reactions will amplify a DNA fragment of 3132 and 2488 bp, respectively, for the NHEJ and HR repairs. Figure 7B shows that no bands were revealed after 35 cycles of PCR reaction with the DNA templates from UM1 cells and from the vector control UM1 transfectants, indicating that these cells are deficient in double-strand DNA break repairs. A band of approximately 3.1 kb was amplified with the DNA template from the antizyme UM1 transfectants and from UM2 cells, demonstrated that the linealized pREC has been repaired by the NHEJ but not the HR mechanism.

DISCUSSION

We have previously reported that antizyme gene expression is diminished in hamster oral cancer cell lines (*15*) and that forced expression of the hamster antizyme gene reversed

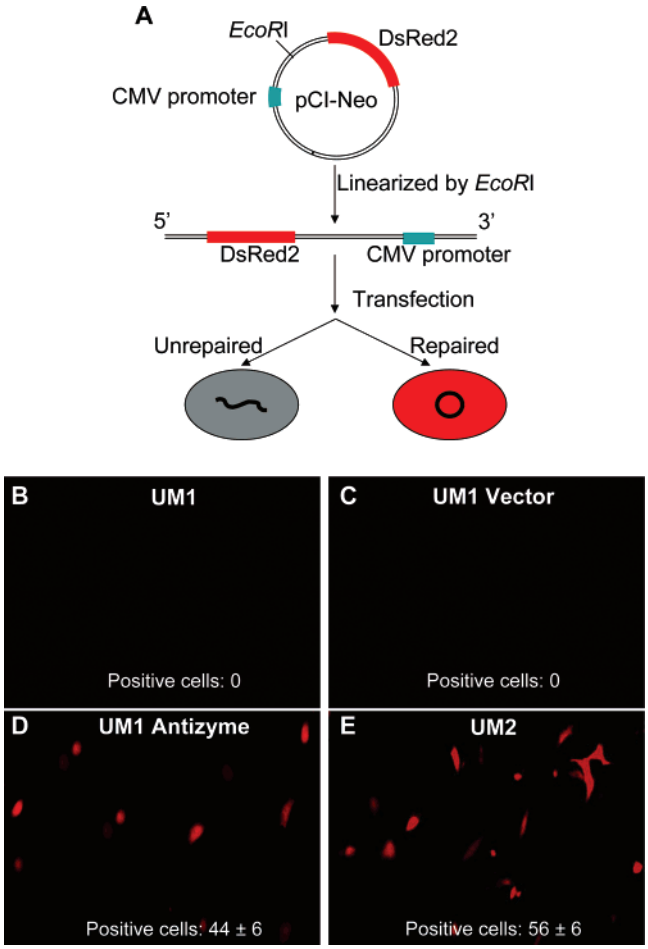

FIGURE 6: Antizyme enhances end-joining activity of DNA double-strand breaks in UM1 cells. A red fluorescent protein (DsRed2) expression vector was constructed by inserting the DsRed2-encoding DNA into the pCI-Neo vector that has been cut by *Sal*I and *Not*I (A). The plasmid was linealized by *Eco*RI digestion and transfected into the UM1 parent cells (B), vector (C) and antizyme (D) UM1 transfectants, and UM2 cells (E) that have been cultured in the presence of 100 μM $ZnSO_4$ for 5 days. Expression of DsRed2 was detected under fluorescent microscopy after 24 h.

the malignant phenotype and induced epithelial differentiation and DNA demethylation (*16*). To identify human genes upregulated by antizyme through DNA demethylation, we compared gene expression profiles of the UM1 human oral squamous cell carcinoma line after 5-Aza-CdR treatment and after ectopic expression of human antizyme. 5-Aza-CdR is a known demethylating reagent (*22*, *23*) that has been used to categorize all of the methylation-silenced genes. Such a comparison identified 39 genes that are commonly upregulated by both antizyme transfection and 5-Aza-CdR treatment. However, the qRT-PCR assay revealed that only 19 of the 39 genes were actually elevated. The remaining 20 genes are thus false positives probably because of the intrinsic defects of the array analysis approach in specificity and reproducibility (*40*). All of the primers used for qRT-PCR have been confirmed to be able to quantify target mRNA and are therefore not a cause for this discrepancy. The array screening method is also prone to false negatives. For example, E-cadherin is known to be expressed in UM1 cells at a significant level and is enhanced by 5-Aza-CdR treatment (*41*), but no detectable signals appeared on the membranes of the BD Atlas Human 3.6 Array. We have also tried two array membranes from another manufacturer (SuperArray),

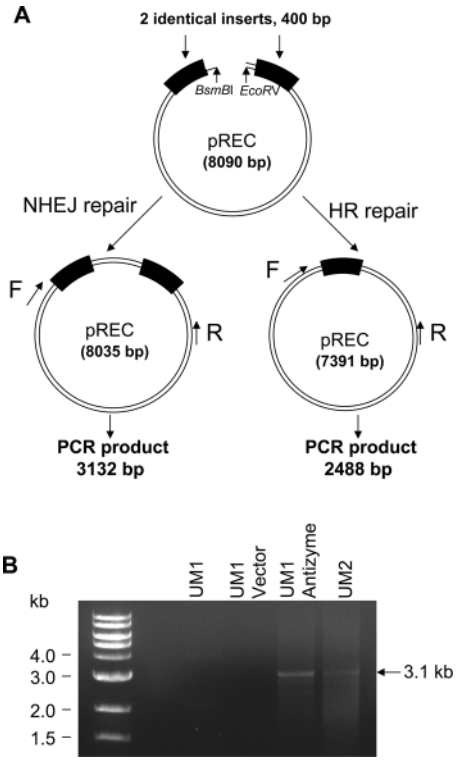

FIGURE 7: Antizyme increases nonhomologous end-joining but not homologous recombination DNA repair activity. (A) NHEJ and HR repair processes in the pREC plasmid-based assay produce PCR fragments of different sizes. (B) pREC was linealized by double digestion with *Bsm*BI and *Eco*RV, transfected into UM1 parent, vector and antizyme UM1 transfectants, and UM2 cells, and cultured for 16 h. DNA were extracted from the transfectants, and PCR reactions were carried out.

the Human Extracellular Matrix and Adhesion Molecules Oligo GEArray and the Human Tumor Metastasis Oligo GEArray, but they also failed to detect E-cadherin signals. More importantly, sequence analyses did not reveal any CpG islands in the promoter regions of the 19 confirmed genes, excluding the possibility that their upregulation by antizyme transfection and by 5-Aza-CdR is directly mediated by DNA demethylation. Thus, our original objective to identify genes upregulated by antizyme through DNA demethylation has failed. While this was disappointing, we found that at least 6 of the 19 confirmed genes are related to the DNA repair function in the G_1 phase (Table 4). For example, DNA−PK, a member of PI-3K-related protein kinases of the ATM/ATR superfamily (*42*, *43*), is implicated in damage sensing as well as double-strand break repair (*37*). It plays a major role in the nonhomologous end-joining DNA repair process (*44*), one of the two major pathways (homologous recombination and nonhomologous end-joining) (*45*) by which DNA double-strand breaks are repaired. Moreover, MCM4 and MCM5 are two essential subunits of the MCM2−MCM7 hexameric complex that plays a key role as a licensing factor in DNA replication. The MCM2−MCM7 proteins, together with Cdc6 and Cdt1, are loaded around the origin recognition complex to form a pre-replication complex as part of the replication licensing machinery during the G_1 phase. Thus, antizyme-mediated upregulation of MCM4 and MCM5 enables the formation of the pre-replication complex that is ready to unwind replication origins. On the other hand, an excess amount of MCM5 has been shown to inhibit the helicase activity of the MCM4/6/7 subcomplex (*46*) and to

arrest cells in the G_1 phase (*47*, *48*). These results are consistent with the significant increase in the G_1 cell population in antizyme transfectants (Table 1).

The findings that antizyme upregulates DNA−PKcs and Ku70 in UM1 cells prompted us to investigate the role of antizyme in DNA double-strand break repairs. Radiosensitivity assay showed that UM1 cells are more sensitive to irradiation-induced damage than UM2 cells (Figure 3). Comet assay indicated that DNA fragmentations are accumulated in UM1 cells even without exogenous stimulation (Figure 4). In both cases, ectopic expression of antizyme restored the ability of UM1 cells to repair DNA damage to the level of UM2 cells. These results demonstrated that antizyme plays a role in maintaining genome integrity and in repairing damaged DNA. This conclusion is supported by the observations that γ-H2AX was accumulated in UM1 cells and that antizyme transfection decreased γ-H2AX foci by 91% (Figure 5).

The Comet assay was performed in neutral pH, which detects mainly double-strand breaks. Two major processes for the repair of double-strand breaks are known in mammalian cells, including homologous recombination and nonhomologous end-joining (*49*−*51*). To repair double-strand breaks by homologous recombination, two types of repair pathways have been established: single-strand annealing and synthesis-dependent strand annealing (*49*). Mre11, Rad50, and Nbs1 complexes (MRN complex) are the major players in these processes (*52*). They are responsible for the initial cleaning and conditioning of DNA double-strand break ends to create the 3′ single-stranded DNA overhang by their ATP-dependent 5′ → 3′ exonuclease activity (*53*). qRT-PCR analysis showed that the expression levels of Rad50 and Nbs11 in UM1 cells are 56 and 30%, respectively, of that in UM2 cells. This is consistent with a diminished activity of UM1 cells in DNA double-strand breaks. Antizyme transfection did not upregulate their expression in UM1 cells, suggesting that antizyme does not modulate the homologous recombination process. This is confirmed by the lack of homologous recombination events in antizyme UM1 transfectants (Figure 7).

Nonhomologous end-joining is another major mechanism in the repair of double-strand breaks in mammalian cells. In this process, Ku70 binds to the broken DNA ends as a heterodimer complex with Ku80. They are translocated inward along the DNA and recruit the catalytic subunit of the enzyme, DNA−PKcs (*54*). DNA−PKcs phosphorylates Ku70/Ku80 proteins as well as DNA−PKcs itself (*55*, *56*). After phosphorylation of DNA−PK, MRN complex proteins are subsequently recruited to the broken sites (*57*). The MRN complex treats double-strand break ends by the exonuclease activity. After the conditioning of DNA ends, XRCC4 and DNA ligase fill-in the DNA gap (*58*). Thus, DNA−PKcs and Ku 70 are essential for the initiation of nonhomologous end-joining repair and are rate-limiting. It has been shown that knockout or knockdown of Ku70 (*59*, *60*) and DNA−PKcs (*61*) resulted in hypersensitivity to radiation. Our results of both pCI-DsRed2 (Figure 6) and pREC (Figure 7) experiments demonstrated that UM1 cells are deficient in both homologous recombination and nonhomologous end-joining and that ectopic expression of antizyme restored the nonhomologous end-joining process. It is unknown at present how antizyme upregulates the genes involved in DNA repairs and whether it interacts directly with DNA−PKcs and Ku70. Nevertheless, the data presented in this paper demonstrated that antizyme enhances the nonhomologous end-joining repair of DNA double-strand breaks through the upregulation of DNA−PKcs and Ku70 in UM1 human oral cancer cells.

ACKNOWLEDGMENT

We thank Drs. S. Mizutani for providing pMT/CB6$^+$ vector and pMT/CB6$^+$HuFSAZ-wt plasmid, T. Kohno for providing pREC plasmid, J. Mitchell for providing anti-antizyme polyclonal antibody, and J. Rheinwald for providing OKF4, OKF6, SCC4, SCC15, SCC66, and SCC105L cells.

REFERENCES

1. Romano, M., Santacroce, M. A., Bonelli, P., Cecco, L., and Cerra, M. (1986) Differences in polyamine metabolism between carcinomatous and uninvolved human breast tissues, *Int. J. Biol. Markers 1*, 77−80.
2. Lundell, L., and Rosengren, E. (1986) Polyamine levels in human gastric carcinoma, *Scand. J. Gastroenterol. 21*, 829−832.
3. Radford, D. M., Nakai, H., Eddy, R. L., Haley, L. L., Byers, M. G., Henry, W. M., Lawrence, D. D., Porter, C. W., and Shows, T. B. (1990) Two chromosomal locations for human ornithine decarboxylase gene sequences and elevated expression in colorectal neoplasia, *Cancer Res. 50*, 6146−6153.
4. Tamori, A., Nishiguchi, S., Kuroki, T., Seki, S., Kobayashi, K., Kinoshita, H., and Otani, S. (1994) Relationship of ornithine decarboxylase activity and histological findings in human hepatocellular carcinoma, *Hepatology 20*, 1179−1186.
5. Pegg, A. E. (1988) Polyamine metabolism and its importance in neoplastic growth and a target for chemotherapy, *Cancer Res. 48*, 759−774.
6. Frostesjo, L., Holm, I., Grahn, B., Page, A. W., Bestor, T. H., and Heby, O. (1997) Interference with DNA methyltransferase activity and genome methylation during F9 teratocarcinoma stem cell differentiation induced by polyamine depletion, *J. Biol. Chem. 272*, 4359−4366.
7. Hayashi, S., Murakami, Y., and Matsufuji, S. (1996) Ornithine decarboxylase antizyme: A novel type of regulatory protein, *Trends Biochem. Sci. 21*, 27−30.
8. Coffino, P. (2001) Antizyme, a mediator of ubiquitin-independent proteasomal degradation, *Biochimie 83*, 319−323.
9. Murakami, Y., Matsufuji, S., Kameji, T., Hayashi, S., Igarashi, K., Tamura, T., Tanaka, K., and Ichihara, A. (1992) Ornithine decarboxylase is degraded by the 26S proteasome without ubiquitination, *Nature 360*, 597−599.
10. Zhu, C., Lang, D. W., and Coffino, P. (1999) Antizyme2 is a negative regulator of ornithine decarboxylase and polyamine transport, *J. Biol. Chem. 274*, 26425−26430.
11. Ivanov, I. P., Rohrwasser, A., Terreros, D. A., Gesteland, R. F., and Atkins, J. F. (2000) Discovery of a spermatogenesis stage-specific ornithine decarboxylase antizyme: Antizyme 3, *Proc. Natl. Acad. Sci. U.S.A. 97*, 4808−4813.
12. Tosaka, Y., Tanaka, H., Yano, Y., Masai, K., Nozaki, M., Yomogida, K., Otani, S., Nojima, H., and Nishimune, Y. (2000) Identification and characterization of testis specific ornithine decarboxylase antizyme (OAZ-t) gene: Expression in haploid germ cells and polyamine-induced frameshifting, *Genes Cells 5*, 265−276.
13. Matsufuji, S., Matsufuji, T., Miyazaki, Y., Murakami, Y., Atkins, J. F., Gesteland, R. F., and Hayashi, S. (1995) Autoregulatory frameshifting in decoding mammalian ornithine decarboxylase antizyme, *Cell 80*, 51−60.
14. Murakami, Y., Matsufuji, S., Nishiyama, M., and Hayashi, S. (1989) Properties and fluctuations in vivo of rat liver antizyme inhibitor, *Biochem. J. 259*, 839−845.
15. Tsuji, T., Todd, R., Meyer, C., McBride, J., Liao, P. H., Huang, M. F., Chou, M. Y., Donoff, R. B., and Wong, D. T. (1998) Reduction of ornithine decarboxylase antizyme (ODC-Az) level in the 7,12-dimethylbenz(*a*)anthracene-induced hamster buccal pouch carcinogenesis model, *Oncogene 16*, 3379−3385.
16. Tsuji, T., Usui, S., Aida, T., Tachikawa, T., Hu, G. F., Sasaki, A., Matsumura, T., Todd, R., and Wong, D. T. (2001) Induction of epithelial differentiation and DNA demethylation in hamster

malignant oral keratinocyte by ornithine decarboxylase antizyme, *Oncogene 20*, 24−33.
17. Feith, D. J., Shantz, L. M., and Pegg, A. E. (2001) Targeted antizyme expression in the skin of transgenic mice reduces tumor promoter induction of ornithine decarboxylase and decreases sensitivity to chemical carcinogenesis, *Cancer Res. 61*, 6073−6081.
18. Bettuzzi, S., Davalli, P., Astancolle, S., Pinna, C., Roncaglia, R., Boraldi, F., Tiozzo, R., Sharrard, M., and Corti, A. (1999) Coordinate changes of polyamine metabolism regulatory proteins during the cell cycle of normal human dermal fibroblasts, *FEBS Lett. 446*, 18−22.
19. Koike, C., Chao, D. T., and Zetter, B. R. (1999) Sensitivity to polyamine-induced growth arrest correlates with antizyme induction in prostate carcinoma cells, *Cancer Res. 59*, 6109−6112.
20. Newman, R. M., Mobascher, A., Mangold, U., Koike, C., Diah, S., Schmidt, M., Finley, D., and Zetter, B. R. (2004) Antizyme targets cyclin D1 for degradation. A novel mechanism for cell growth repression, *J. Biol. Chem. 279*, 41504−41511.
21. Nakayama, S., Sasaki, A., Mese, H., Alcalde, R. E., and Matsumura, T. (1998) Establishment of high and low metastasis cell lines derived from a human tongue squamous cell carcinoma, *Invasion Metastasis 18*, 219−228.
22. Juttermann, R., Li, E., and Jaenisch, R. (1994) Toxicity of 5-aza-2′-deoxycytidine to mammalian cells is mediated primarily by covalent trapping of DNA methyltransferase rather than DNA demethylation, *Proc. Natl. Acad. Sci. U.S.A. 91*, 11797−11801.
23. Christman, J. K. (2002) 5-Azacytidine and 5-aza-2′-deoxycytidine as inhibitors of DNA methylation: Mechanistic studies and their implications for cancer therapy, *Oncogene 21*, 5483−5495.
24. Iwata, S., Sato, Y., Asada, M., Takagi, M., Tsujimoto, A., Inaba, T., Yamada, T., Sakamoto, S., Yata, J., Shimogori, T., Igarashi, K., and Mizutani, S. (1999) Anti-tumor activity of antizyme which targets the ornithine decarboxylase (ODC) required for cell growth and transformation, *Oncogene 18*, 165−172.
25. Chirgwin, J. M., Przybyla, A. E., MacDonald, R. J., and Rutter, W. J. (1979) Isolation of biologically active ribonucleic acid from sources enriched in ribonuclease, *Biochemistry 18*, 5294−5299.
26. Asaumi, J., Higuchi, Y., Murakami, J., Kuroda, M., Shibuya, K., Konouchi, H., Hisatomi, M., Matsuzaki, H., Shigehara, H., Kawasaki, S., Kishi, K., and Hiraki, Y. (2002) Thermoradiotherapy in human head and neck squamous cell carcinoma cell lines, *Int. J. Mol. Med. 10*, 287−291.
27. Lemay, M., and Wood, K. A. (1999) Detection of DNA damage and identification of UV-induced photoproducts using the CometAssay kit, *BioTechniques 27*, 846−851.
28. Angelis, K. J., Dusinska, M., and Collins, A. R. (1999) Single cell gel electrophoresis: Detection of DNA damage at different levels of sensitivity, *Electrophoresis 20*, 2133−2138.
29. Zhong, Q., Chen, C. F., Chen, P. L., and Lee, W. H. (2002) BRCA1 facilitates microhomology-mediated end joining of DNA double strand breaks, *J. Biol. Chem. 277*, 28641−28647.
30. Sasaki, S., Sato, M., Katsura, Y., Kurimasa, A., Chen, D. J., Takeda, S., Kuwano, H., Yokota, J., and Kohno, T. (2006) Rapid assessment of two major repair activities against DNA double-strand breaks in vertebrate cells, *Biochem. Biophys. Res. Commun. 339*, 583−590.
31. Kim, S. W., Mangold, U., Waghorne, C., Mobascher, A., Shantz, L., Banyard, J., and Zetter, B. R. (2006) Regulation of cell proliferation by the antizyme inhibitor: Evidence for an antizyme-independent mechanism, *J. Cell Sci. 119*, 2583−2591.
32. Eckmann, L., Smith, J. R., Housley, M. P., Dwinell, M. B., and Kagnoff, M. F. (2000) Analysis by high density cDNA arrays of altered gene expression in human intestinal epithelial cells in response to infection with the invasive enteric bacteria *Salmonella*, *J. Biol. Chem. 275*, 14084−14094.
33. Gross, C., Kelleher, M., Iyer, V. R., Brown, P. O., and Winge, D. R. (2000) Identification of the copper regulon in *Saccharomyces cerevisiae* by DNA microarrays, *J. Biol. Chem. 275*, 32310−32316.
34. Pietiainen, V., Huttunen, P., and Hyypia, T. (2000) Effects of echovirus 1 infection on cellular gene expression, *Virology 276*, 243−250.
35. Hu, D., Cao, K., Peterson-Wakeman, R., and Wang, R. (2002) Altered profile of gene expression in rat hearts induced by chronic nicotine consumption, *Biochem. Biophys. Res. Commun. 297*, 729−736.
36. Ranganna, K., Yousefipour, Z., Yatsu, F. M., Milton, S. G., and Hayes, B. E. (2003) Gene expression profile of butyrate-inhibited vascular smooth muscle cell proliferation, *Mol. Cell. Biochem. 254*, 21−36.
37. Gottlieb, T. M., and Jackson, S. P. (1993) The DNA-dependent protein kinase: Requirement for DNA ends and association with Ku antigen, *Cell 72*, 131−142.
38. Jackson, S. P. (2001) Detecting, signalling and repairing DNA double-strand breaks, *Biochem. Soc. Trans. 29*, 655−661.
39. Norbury, C. J., and Hickson, I. D. (2001) Cellular responses to DNA damage, *Annu. Rev. Pharmacol. Toxicol. 41*, 367−401.
40. Larkin, J. E., Frank, B. C., Gavras, H., Sultana, R., and Quackenbush, J. (2005) Independence and reproducibility across microarray platforms, *Nat. Methods 2*, 337−344.
41. Nakayama, S., Sasaki, A., Mese, H., Alcalde, R. E., Tsuji, T., and Matsumura, T. (2001) The E-cadherin gene is silenced by CpG methylation in human oral squamous cell carcinomas, *Int. J. Cancer 93*, 667−673.
42. Hartley, K. O., Gell, D., Smith, G. C., Zhang, H., Divecha, N., Connelly, M. A., Admon, A., Lees-Miller, S. P., Anderson, C. W., and Jackson, S. P. (1995) DNA-dependent protein kinase catalytic subunit: A relative of phosphatidylinositol 3-kinase and the ataxia telangiectasia gene product, *Cell 82*, 849−856.
43. Poltoratsky, V. P., Shi, X., York, J. D., Lieber, M. R., and Carter, T. H. (1995) Human DNA-activated protein kinase (DNA−PK) is homologous to phosphatidylinositol kinases, *J. Immunol. 155*, 4529−4533.
44. Lee, S. E., Mitchell, R. A., Cheng, A., and Hendrickson, E. A. (1997) Evidence for DNA−PK-dependent and -independent DNA double-strand break repair pathways in mammalian cells as a function of the cell cycle, *Mol. Cell. Biol. 17*, 1425−1433.
45. Ferguson, D. O., Sekiguchi, J. M., Chang, S., Frank, K. M., Gao, Y., DePinho, R. A., and Alt, F. W. (2000) The nonhomologous end-joining pathway of DNA repair is required for genomic stability and the suppression of translocations, *Proc. Natl. Acad. Sci. U.S.A. 97*, 6630−6633.
46. Sato, M., Gotow, T., You, Z., Komamura-Kohno, Y., Uchiyama, Y., Yabuta, N., Nojima, H., and Ishimi, Y. (2000) Electron microscopic observation and single-stranded DNA binding activity of the Mcm4,6,7 complex, *J. Mol. Biol. 300*, 421−431.
47. Zhang, J. J., Zhao, Y., Chait, B. T., Lathem, W. W., Ritzi, M., Knippers, R., and Darnell, J. E., Jr. (1998) Ser727-dependent recruitment of MCM5 by Stat1α in IFN-γ-induced transcriptional activation, *EMBO J. 17*, 6963−6971.
48. Ishimi, Y. (1997) A DNA helicase activity is associated with an MCM4, -6, and -7 protein complex, *J. Biol. Chem. 272*, 24508−24513.
49. Helleday, T. (2003) Pathways for mitotic homologous recombination in mammalian cells, *Mutat. Res. 532*, 103−115.
50. Collis, S. J., DeWeese, T. L., Jeggo, P. A., and Parker, A. R. (2005) The life and death of DNA−PK, *Oncogene 24*, 949−961.
51. Burma, S., Chen, B. P., and Chen, D. J. (2006) Role of non-homologous end joining (NHEJ) in maintaining genomic integrity, *DNA Repair (Amsterdam) 5*, 1042−1048.
52. Jackson, S. P. (2002) Sensing and repairing DNA double-strand breaks, *Carcinogenesis 23*, 687−696.
53. Assenmacher, N., and Hopfner, K. P. (2004) MRE11/RAD50/NBS1: Complex activities, *Chromosoma 113*, 157−166.
54. Walker, J. R., Corpina, R. A., and Goldberg, J. (2001) Structure of the Ku heterodimer bound to DNA and its implications for double-strand break repair, *Nature 412*, 607−614.
55. Gell, D., and Jackson, S. P. (1999) Mapping of protein−protein interactions within the DNA-dependent protein kinase complex, *Nucleic Acids Res. 27*, 3494−3502.
56. Chan, D. W., Ye, R., Veillette, C. J., and Lees-Miller, S. P. (1999) DNA-dependent protein kinase phosphorylation sites in Ku 70/80 heterodimer, *Biochemistry 38*, 1819−1828.
57. Weterings, E., and van Gent, D. C. (2004) The mechanism of non-homologous end-joining: A synopsis of synapsis, *DNA Repair (Amsterdam) 3*, 1425−1435.
58. Grawunder, U., Wilm, M., Wu, X., Kulesza, P., Wilson, T. E., Mann, M., and Lieber, M. R. (1997) Activity of DNA ligase IV stimulated by complex formation with XRCC4 protein in mammalian cells, *Nature 388*, 492−495.
59. Omori, S., Takiguchi, Y., Suda, A., Sugimoto, T., Miyazawa, H., Tanabe, N., Tatsumi, K., Kimura, H., Pardington, P. E., Chen,

F., Chen, D. J., and Kuriyama, T. (2002) Suppression of a DNA double-strand break repair gene, Ku70, increases radio- and chemosensitivity in a human lung carcinoma cell line, *DNA Repair (Amsterdam) 1*, 299−310.

60. Ayene, I. S., Ford, L. P., and Koch, C. J. (2005) Ku protein targeting by Ku70 small interfering RNA enhances human cancer cell response to topoisomerase II inhibitor and γ radiation, *Mol. Cancer Ther. 4*, 529−536.
61. Peng, Y., Zhang, Q., Nagasawa, H., Okayasu, R., Liber, H. L., and Bedford, J. S. (2002) Silencing expression of the catalytic subunit of DNA-dependent protein kinase by small interfering RNA sensitizes human cells for radiation-induced chromosome damage, cell killing, and mutation, *Cancer Res. 62*, 6400−6404.

BI7000328